Room Temperature Optically Detected Magnetic Resonance of Triplet Excitons in a Pentacene-doped Picene Single Crystal.

Fabrizio Moro, Massimo Moret, Alberto Ghirri, Andrés Granados del Águila, Yoshihiro Kubozono, Luca Beverina, Antonio Cassinese*

Dr. F. Moro, Prof. M. Moret, Prof. L. Beverina.
Department of Materials Science, University of Milano-Bicocca, via Cozzi 55, Milan I-20125, Italy
E-mail: fabrizio.moro@unimib.it

Dr. A. Ghirri
Istituto Nanoscienze - CNR, via Campi 213/a, Modena I-41125, Italy

Dr. A. Granados del Águila
Division of Physics and Applied Physics, School of Physical and Mathematical Sciences, Nanyang Technological University, Singapore.

Prof. Y. Kubozono
Research Institute for Interdisciplinary Science, Okayama University, Okayama 700-8530, Japan

Prof. A. Cassinese
Department of Physics "Ettore Pancini", University of Naples 'Federico II', Piazzale Tecchio, 80, Naples I-80125, Italy

Keywords: organic semiconductors, pentacene, picene, electron spin resonance, optically detected magnetic resonance, delayed fluorescence, triplet excitons, MASER

The inclusion of functional molecules as substitutional dopants in single crystals of organic hosts with complementary optical properties provides a versatile strategy to tune optical and magnetic properties in view of their applications in optoelectronics and spintronics. Here, by combining electron spin resonance and optical spectroscopy, isolated triplet exciton states with distinct emission and absorptive resonance modes from two magnetically inequivalent sites of pentacene within the picene crystal could be detected at room temperature. This is possible due to the incorporation of a low-doping, 1% mol/mol of pentacene into the monoclinic polymorph of picene high-quality single crystals. In addition, we demonstrate optically detected magnetic resonance (ODMR) due

to delayed fluorescence. Our findings demonstrate that isolated pentacene molecules in picene matrices show efficient spin-dependent optical activities that are tuned by crystallographically oriented magnetic fields. These properties are particularly appealing for the exploitation of pentacene in room temperature spin-driven opto-electronics, quantum sensing and in microwave amplification by stimulated emission of radiation (MASER).

Introduction

The preparation of mixed organic crystals provides multifunctional optical, electronic and magnetic properties embedded within the same material system offering opportunities in organic based devices for applications in optoelectronics[1] and spintronics[2]. The isolation of guest molecules within a host matrix and control of their concentration enable a fine tuning of the intermolecular couplings which in turn may lead to the observation of interesting physical phenomena such as i) enhanced singlet fission efficiency[3, 4], ii) isolation of optically excited triplet states robust against decoherence,[5] iii) energy transfer and up or down energy conversion.[6, 7]

π-conjugated organic materials based on aromatic building blocks such as acenes[8] and phenacenes[9] are at the forefront of current research because they show remarkable photonic and electronic properties.[10-12] Pentacene is one of the most investigated organic molecules within the acene family because of its large spin polarization, long-living optically excited triplet state via intersystem crossing (ISC) at room temperature[8, 13, 14] and long spin coherence time.[15] The optical properties of pentacene doped *p*-terphenyl single crystals and films have been widely investigated as benchmark for single molecule spectroscopy,[16] charge transfer and Frenkel excitons,[14] quantum sensing,[17] single fission[4] and MASER applications by exploiting the inversion of population of the pentacene triplet state.[18] Doping of pentacene in naphthalene has enabled dynamic nuclear polarization as high as 94%.[19-21] In addition, pentacene shows hole mobility comparable to those of amorphous inorganic materials[22, 23] and efficient singlet exciton fission.[24-26]

Phenacenes are noncentrosymmetric versions of acenes consisting of rings fused in angular-oriented structures.[11, 27] Among the phenacene series, picene is the closest structural isomer

to pentacene with similar molecular volume and length. These properties make picene the most natural choice for hosting substitutional pentacene molecules. In addition, unlike pentacene, picene is soluble in many common organic solvents and shows intrinsic stability larger than pentacene under atmospheric conditions due to the armchair edges conformation (symmetry: C_{2v}), deep HOMO level (-5.5 eV) and large band gap (~ 3.3 eV).[14] However, the synthesis of phenacenes is less efficient than acenes, as such the studies of their physical properties has progressed at slower pace.[12] Nevertheless, picene has recently attracted a large interest after the discovery of superconductivity[12, 14, 28] and transport properties for field effect transistors both as thin films[9, 29, 30] and heterostructures.[31]

Although pentacene and picene are structural isomers, they show significantly different electronic[32] and optical[11] properties due to the different arrangements of the rings and energy levels misalignment resulting in an overlap between the pentacene absorption spectrum with the picene photoluminescence.[33] So far, doping of picene with pentacene has been realized only in films studied by light-absorption and photoluminescence, which have shown robust singlet fission by controlling the spacing between pentacene molecules in a picene matrix[3] and efficient energy transfer from picene to pentacene in films grown by supersonic beams.[14, 33]

Therefore, picene molecules provide a more advantageous host-material for pentacene compared to other organic molecules because: i) protect and isolate pentacene molecules from the environment and from the triplet-triplet interactions, and ii) provide a means to extend the excitation of pentacene in the ultraviolet region of the electromagnetic spectrum by picene to pentacene energy transfer.[33] The latter mechanism could be exploited in other suitable combinations of phenacenes and acenes with complementary optical properties, thus opening up the possibility to populate excitonic triplet states by ISC according to the spin statistics under low laser power which otherwise would damage the material.

To the best of our knowledge no single crystals of pentacene-doped picene have been reported, and the magnetic anisotropy of the pentacene triplet exciton states in a picene host remains unknown. Furthermore, studies on films of pentacene-doped picene have mainly focused on photoluminescence and absorption measurements. However, by combining optical excitation and detection with electron spin resonance (ESR) it is possible to spectroscopically probe and manipulate the energy level populations of the triplet state.

Herein, we report on the spin-dependent optical properties of a pentacene-doped picene single crystal studied by photo-ESR and optically detected magnetic resonance (ODMR). We investigate the magnetic anisotropy and the hyperfine couplings of the excitonic triplet as well as the angular dependence of the light-induced emissive and absorptive resonance modes of the optically detected magnetic resonances. Finally, time-resolved photoluminescence experiments provide compelling evidences that the ODMR signal originates from delayed fluorescence involving optically excited triplets. Our findings demonstrate efficient spin-dependent optical activities of pentacene triplet excitons in a picene matrix. In particular we observe room temperature and long living optically spin polarized states of pentacene triplet excitons which can be tuned by cryptographically oriented magnetic fields on a wide time scale spanning up to milliseconds. Our results shed light on the potential applications of pentacene-doped picene crystals in spin-driven opto-electronics.

Materials and Methods

X-ray Diffraction: Red-pink single crystals of pentacene-doped picene suitable for a full physical characterization were obtained via the vertical Bridgman-Stockbarger method. A vial of borosilicate glass (internal diameter, 10 mm; height, 70 mm) was charged with a mixture of pentacene and picene in a stoichiometric ratio of approximately 1:100 mol/mol. Owing to oxygen contamination during growth, the actual concentration of pentacene surviving in the crystal may have been somewhat lower than this. The vial was flame sealed under reduced pressure (0.01 atm) and lowered through a vertical tube furnace set at 380°C at a rate of 3 mm h^{-1}. A clean, pink crystal sample of ca. 40 mm length formed, gradually fracturing on cooling to room temperature at a rate of approximately 10 °C h^{-1}. The vial was cracked open, and the crystal sample removed almost intact from it. A single crystalline shard of approximately 5 mm length and prismoid shape was carefully removed from the bulk sample by gently pulling across a clear crystalline fracture. Such a sample was checked with a Rigaku R-Axis II X-ray diffractometer at room temperature with Mo-Kα radiation.

Molecular Dynamics: Molecular dynamics (MD) simulations were performed to model the orientation of isolated pentacene molecules doping picene crystals. Unit cell parameters and crystal structure of monoclinic picene were taken from reference[34]. The molecular structure of pentacene was extracted from reference.[35] One molecule of pentacene was introduced as a substitutional defect within the 240 molecules of the MD simulation box. A supercell

consisting of 5×6×4 unit cells along the *a, b* and *c* axes was employed to describe the picene crystal with three-dimensional periodic boundary conditions. Simulations were performed using the TINKER8.8.3 package[36] under constant temperature and pressure conditions (NPT), with a duration of 0.5 ns. The force field was OPLS-AA[37, 38] with parameters for bonding and non-bonding interactions for aromatic carbon and hydrogen atoms. Non-bonded interactions were cutoff at 1.8 nm. The Verlet algorithm with a time step of 1 fs was used to integrate the equations of motion. The pressure was maintained constant (1 atm) with a Berendsen barostat, with a coupling constant of 1.0 ps. The temperature was controlled with a Berendsen thermostat and a time constant of 0.1 ps. Relevant observables extracted after equilibration included mass centroids, tilt angle defined by means of the pentacene x molecular axis in **Figure 1b** with respect to the *ab* plane of picene, and Euler angles according to the molecular reference frame of **Figure 1b** with respect to the unit cell axes of picene *a*, *b* and *c** taken as the fixed frame reference *x, y* and *z*, respectively.

Optically Detected Magnetic Resonance and Photo-Electron Spin Resonance: ODMR spectra were recorded at room temperature in a Bruker ELEXYS X-band (9.8 GHz) spectrometer. A shard of a single crystal of picene:pentacene was glued on a flat-shaped end of a quartz tube and inserted into a super high-Q rectangular resonator placed in between the poles of an electromagnet and provided with a front grid to allow optical access and of a goniometer for fine sample rotation (~ 1°) with respect to the external magnetic field, *B*. The crystal was rotated around the *a* crystal axis from *B* parallel to *c* to *B* parallel to *b*. The rotation of the crystal around the *c* axis, is particularly challenging due to the reduced crystal size to fit the ESR sample support and the low signal-to-noise-ratio. A Coherent - Verdi laser was used to excite the pentacene $S_0 \rightarrow S_1$ transition within the picene single crystal with wavelength $\lambda = 532$ nm and power $P = 500$ mW. The photoluminescence signal was filtered with a 550 nm long pass filter transparent to Stokes-shifted fluorescence emission, detected by a silicon detector, amplified by a low-noise Stanford SR560 preamplifier and lock-in demodulated by a square-wave modulated microwave excitation with amplitude of ~ 2 W and frequency of 1 KHz. For photo-ESR measurements the spectra were recorded by demodulating the reflected signal from the resonant cavity upon microwave sample absorption by a small oscillating magnetic field with amplitude of 0.1 mT and frequency of 100 KHz. Due to an impurity present in the cavity of the Bruker spectrometer in the spectral region of g ~ 2, continuous wave-ESR spectra were recorded on a super-high Q cavity of a Varian spectrometer free of contaminations. All spectra

and resonance field road maps were recorded at room temperature and simulated with the *Easyspin* software.[39]

*Fluorescence and Time Resolved Fluorescence***:** Optical spectra at room temperature were recorded on an ensemble of pentacene-doped picene single crystals in an Agilent Technologies Cary Eclipse Fluorescence Spectrophotometer equipped with a Xenon lamp with output power of 15 W and a photomultiplier tube (PMT) for detection. Photoluminescence excitation was recorded by detecting the emission at λ_{em} = 645 nm and by scanning the excitation wavelength in the range λ_{exc} = 300 - 600 nm.

Fluorescence and delayed fluorescence were detected with the same λ_{exc} = 532 nm and spectral emission range λ_{exc} = 580 - 800 nm except that for the dFL the emitted signal was detected after a delay time of 100 μs and integrated for 200 ms with gate time of 5 ms. Lifetime measurements were recorded with the following parameters: λ_{ex} = 532 nm, λ_{em} = 645 nm and several delay times to cover a time range of 10^0 – 10^5 μs. Cutt-off and optical density filters were used in excitation and detection, for both PL and time-resolved experiments.

Results and discussion

Figure 1a shows the crystal structure of picene with views along the *c* and *b* crystallographic axis. From the X-ray diffraction data we obtained unit cell parameters a = 8.352(19) Å, b = 6.347(13) Å, c = 13.553(20) Å, β = 90.07(13)°, in space group $P2_1$ (no. 4), which are in agreement with the monoclinic polymorph of pure picene.[34, 40, 41] In analogy with what was previously observed in *p*-terphenyl:pentacene crystals, one can assume that the pentacene molecule is substitutional to one of the two *ca*. 60° apart crystallographic equivalent sites of picene, than can take one of these two orientations.[42] In this configuration, the molecular x axis has a unique orientation for all sites, whereas the y and z axis are tilted by 58.37° with respect to each other. The different arrangement of the rings of pentacene and picene (**Figure 1b**) results in a wider band gap for picene compared to pentacene and favourable alignment of the singlet energy levels for efficient energy transfer (**Figure 1c**).[43]

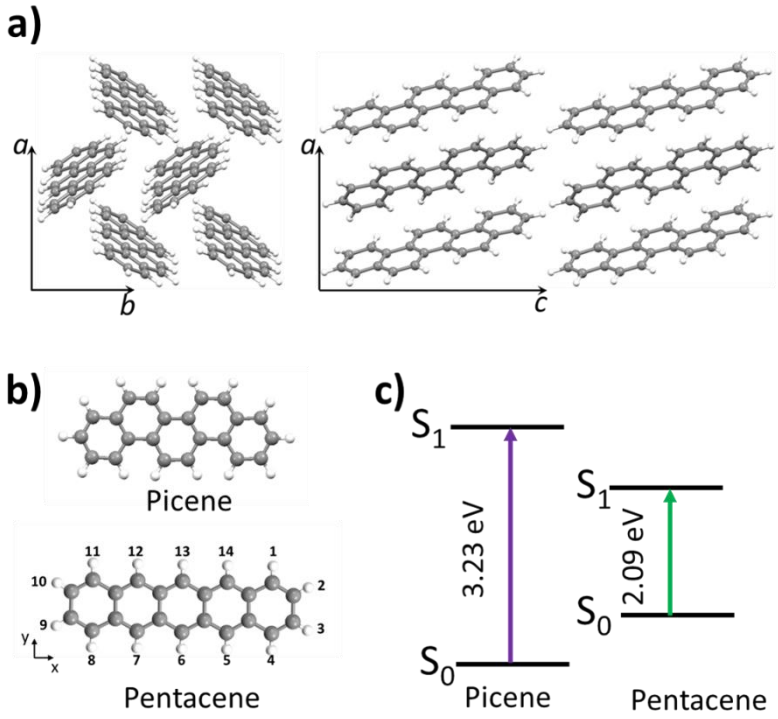

Figure 1 a) Views along the *c* and *b* crystallographic axis of a picene single crystal. Colour code: white is for hydrogen atoms and grey for carbon atoms. **b)** Structures of the picene and pentacene molecules. **c)** Relative energy levels of picene and pentacene.

Figure 2a shows the orientation of a pentacene substitutional molecule relative to the picene crystal axes and to the external magnetic field **B** which is rotated by the angle θ around the *a* axis, whereas **Figures 2b** reports the light-induced or photo-electron spin resonance (photo-ESR) spectra of a pentacene doped picene single crystal recorded at room temperature for an arbitrary angle, $\theta = 64°$. The spectrum shows two pairs of first-derivative resonance lines with an EEAA (where E stands for emission and A for absorption) pattern centred around the *g*-value = 2, with average full-width-half-maximum (FWHM) linewidth of ~ 3 mT and unresolved hyperfine splitting. The inner and outer lines are separated by ~ 28 mT and ~ 52 mT respectively. The first derivative lines are slightly asymmetric due to the rapid passage effect which leads to the dominance of the positive and negative contributions of the first derivative signal for the low and high field peaks respectively. The four resonance lines follow a specific path under rotation of the crystal around the *a* axis (**Figure 2**). The low and high field resonances show a dominant positive (white) and negative (black) contributions respectively for $\theta = 90°$ which reverse for $\theta < 40°$.

cw-ESR and photo-ESR narrow magnetic field scans around $g = 2$ and for the lowest field line are reported in **Figure 2e** and **2f**, respectively. The lowest field resonance reveals 5 equally spaced features whereas the central line has a Lorentzian lineshape with FWHM = 0.4 mT whose resonance field, linewidth and intensity are independent upon laser excitation.

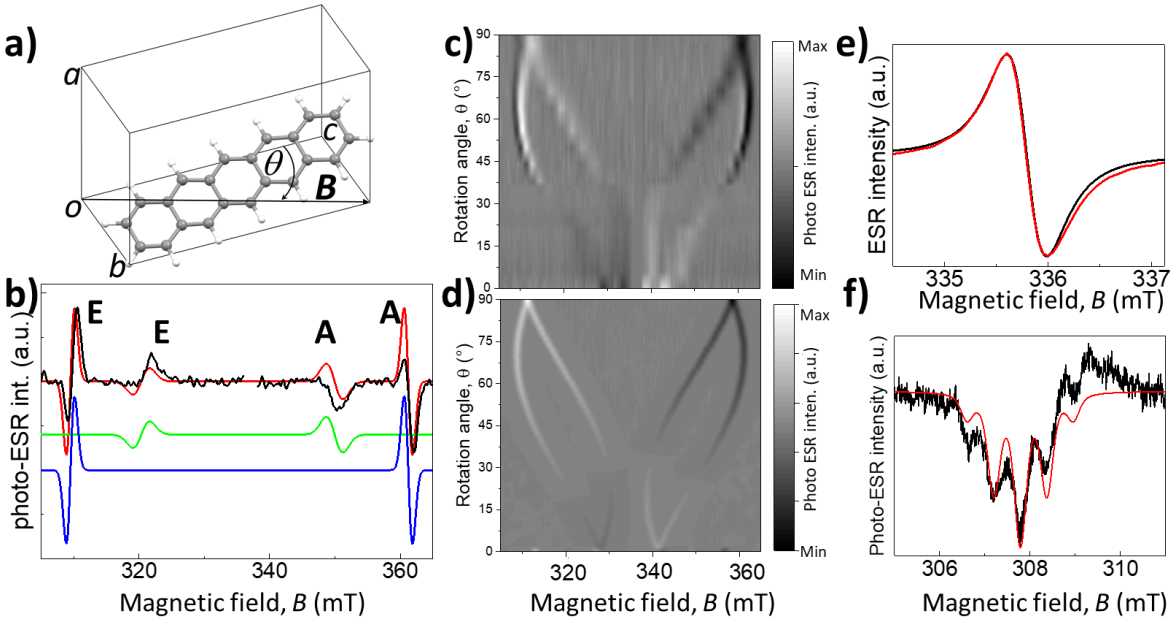

Figure 2 (a) Sketch of the experimental geometry used with the rotation angle θ of the magnetic field relative to the molecular and crystal frames. **b)** Photo-ESR spectra recorded at room temperature for $\theta = 64°$ and the corresponding global spectrum simulation (red curve) with the two magnetically inequivalent components in D_{2h} symmetry (green and blue curves). The emissive (E) and absorptive (A) resonance modes are indicated. Road map of the experimental photo-ESR resonance fields **(c)** and their simulations **(d)**. The colour bar indicates the maximum (white) and minimum (black) intensities in arbitrary units. **e)** Narrow magnetic field scan showing the resonance line at $g \sim 2$ in dark condition along with the simulation. **f)** Photo-ESR spectrum for $\theta = 80°$ showing the resolved hyperfine splitting due to four equivalent protons. The red curve is the simulation to **Equation 1**.

ODMR spectra for the canonical orientations $\theta \sim 0°$ and 90° are shown in **Figure 3a** whereas in **Figure 3b** is reported a contour map of the angular dependent ODMR contrast = ΔPL/PL, where ΔPL is the difference between the photoluminescence signal on and off magnetic resonance condition at a given angle and PL is the off-resonance photoluminescence intensity. The map shows the evolution of ΔPL/PL as function of B and of the angle θ. The two resonances observed for $\theta = 90°$ reach the maximum contrast of about 15%, for $\theta < 90°$ they split in four lines and their resonance fields evolve in a similar fashion as reported for the photo-

ESR spectra in **Figure 2c**. The ODMR contrast decreases steeply for $\theta < 50°$ until it vanishes and reappears for $\theta \sim 0°$ where the four lines tend to merge close to the free electron *g*-value.

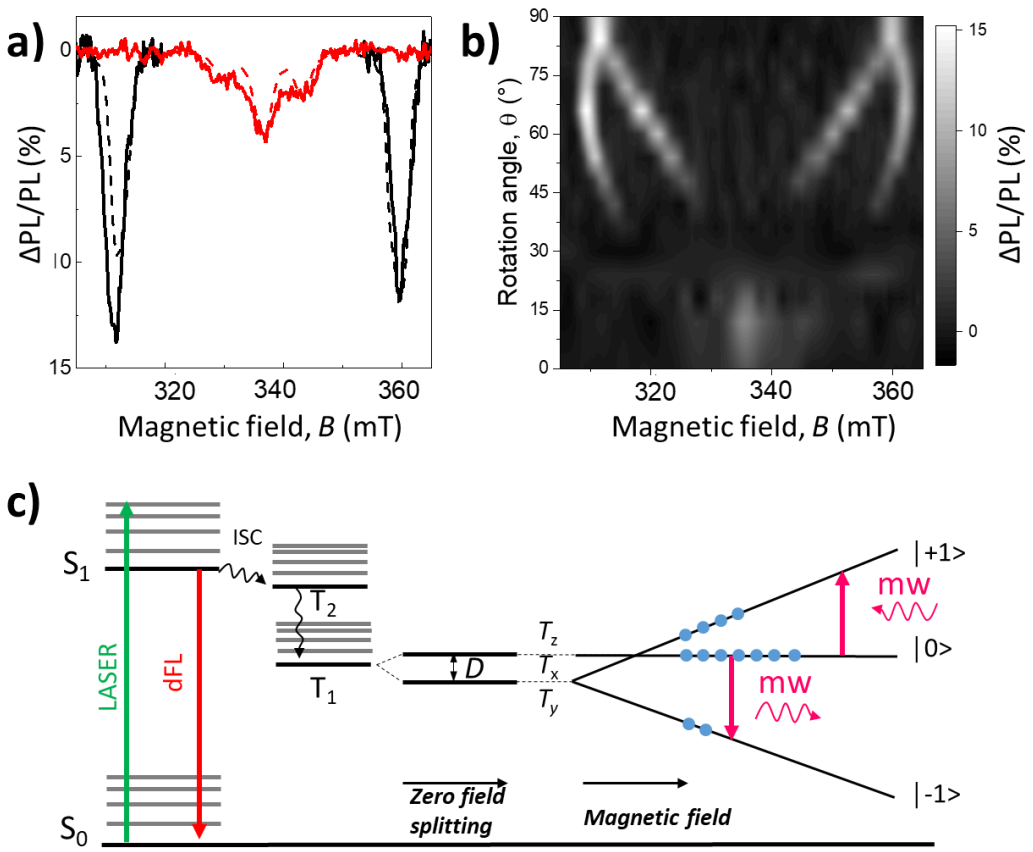

Figure 3 a) ODMR spectra recorded for θ = 90° (black line) and 0° (red line) and the corresponding simulations (dashed lines). **b)** Map of the ODMR contrast as function of the magnetic field and the rotation angle. The colour bar indicates the ODMR contrast percentage. **c)** Jablonski energy level scheme, for the magnetic field direction parallel to the molecular z axis, indicating the intersystem crossing (ISC) with the transfer after internal conversion to the triplet exciton state T_1 sublevels split by zero-field splitting and Zeeman energy in |0>, |+1> and |-1>. The arrows indicate the photon absorption from the S_0 ground state to the singlet S_1 excited state (green), the Stoke-shifted emission (red) and the microwave (mw) induced transitions (purple). The circles represent the relative population of energy levels of the triplet exciton.

Photo-ESR and ODMR offer different advantages in the study of triplet exciton states in organic materials and enable to understand different aspects of the same physical process. More specifically, ODMR enables to detect the changes of the photoluminescence under magnetic resonance condition, as such it is sensitive to spin dependent properties of optical signals. However, due to the selection rules, only optical transitions from energy levels with the same spin quantum number are allowed. In the case of pentacene, when the optical transition S_0 →

S_1 is excited, the system evolves by populating the triplet exciton states from T_N to T_1 manifolds by spin-orbit coupling mediated by ISC, where T_1 is the lowest N state in energy (**Figure 3c**). The zero-field splitting, *D*, splits the T_1 state in the substates denoted as T_z, T_x and T_y whose order depends on the molecular symmetry and sign of *D*.[44] Due to the selection rules, ODMR is mainly sensitive to the variations of the population of the T_z level[45] as such it does not allow to distinguish between absorptive (A) and emissive (E) modes of the transitions within the Zeeman split triplet states. On the contrary, photo-induced ESR is based on the variation of the cavity Q-value induced by emission of absorption of microwave photons stored into the cavity. Because of the phase sensitive lock-in detection and magnetic field modulation, a first derivative spectral lineshape is recorded. The sign of the first-derivative lines provides direct evidence for the observation of the emission and absorptive modes. Photo-ESR is sensitive to the out-equilibrium population of the Zeeman split T_1 energy levels.

We simulate the photo-ESR and ODMR spectra of **Figures 2c** and **3a** with the spin-Hamiltonian:

$$\hat{H} = g\mu_B \mathbf{B}\hat{\mathbf{S}} + DS_z^2 + \sum_i \hat{\boldsymbol{S}} A_i \hat{\boldsymbol{I}}, \quad (1)$$

where *g* is the spectroscopic *g*-value, μ_B is the Bohr magneton, $\boldsymbol{B}$ is the magnetic field vector, $\hat{\boldsymbol{S}}$ and $\hat{\boldsymbol{I}}$ are the electron and nuclear spin operators, *D* is the zero-field splitting and A_i is the hyperfine splitting between the triplet exciton and the *i*-th nuclei. The best fit was obtained for $S = 1$, $D = 1.46$ GHz, $g = 2$ and assuming non-Boltzmann population of the T_1 states in zero-field $P_{Tx} < P_{Ty} < P_{Tz}$ as well as assuming a $P2_1$ symmetry which provides two magnetically inequivalent sites corresponding to the outer and inner resonance pairs respectively (**Figure 2b**). These findings agree with the two sites tilted by 60° with respect to each other at room temperature of pentacene substitutional to picene within the crystal.[42] The hyperfine coupling contribution will be discussed later.

The fit of the spectral contour plot in **Figure 2d** allows the determination of the crystal rotation axes and set the constrains for *D* tensor frame relative to the molecular frame and the latter relative to the picene crystal and laboratory frames. The D_{2h} symmetry of pentacene makes the *D* tensor frame to coincide with the molecular frame[46] which, according to our molecular dynamics (MD) simulation (see Experimental Section), is rotated by the Euler angles $\alpha = 26°$, $\beta = 77°$ and $\gamma = -3°$ with respect to the crystal frame.[42] We obtain a good fit of the road map with the Euler angles $\alpha' = 12°$, $\beta' = 60°$ and $\gamma' = 0°$ (**Figure 2d**), thus suggesting that pentacene molecules substitute picene within the crystal in one of the two sites and that the different conformation of pentacene with respect to picene makes the former to find a slightly different

orientation within the crystal to minimize its potential energy. The molecular *x* axis is the same for all the sites within the crystal, whereas the *y* and *z* axes of the two pentacene sites are not parallel to each other, and cause the appearance of four resonance lines for an arbitrary angle upon rotation of the crystal around the *a* axis. The coincidence of the inner and outer resonance fields obtained for $\theta \sim 0°$ and 90° indicates that **B** is parallel and perpendicular to the molecular *x* axis, respectively (**Figure 2a**). We also expect to observe two resonance lines occurring at a magnetic field spectral separation of 2*D*, however their intensities are below the noise level and could not be observed. In addition, the estimated value for $D = 1.45$ GHz matches well the values previously reported for pentacene in other host matrixes, and it differs significantly from the value $D = 2.7$ GHz reported for picene in *p*-terphenyl.[47] On the other hand, the EEAA pattern observed in the photo-ESR spectra for pentacene in picene is similar for the pentacene in *p*-terphenyl but different from the EAEA observed for pentacene in benzoic acid, thus revealing the influence of the host matrix in determining the inversion of the population.[48]

The emissive (white) and absorptive (black) modes of the photo-ESR resonance lines in **Figure 2c** are well reproduced by the spectral simulations made by integrating the calculated ESR intensities. In particular, we note that the positive and negative signals decrease in intensities by rotating the crystal away from $\theta = 90°$ until they vanish and switch for $\theta \sim 40°$. We ascribe this behaviour to the mixing of the m_s states which breaks the ESR selection rules leading to a decrease of the transition probabilities and to a redistribution of the population of the energy levels. This is an interesting feature because emissive and absorptive modes can be selected both by magnetic field intensity and orientation with respect to the molecular or crystal frame. The ESR signal observed in dark conditions (**Figure 2e**) can be fitted satisfactorily with a Gaussian function with FWHM = 0.66 mT. We ascribe this dark ESR signal to the formation of polarons in the picene-pentacene system where picene acts as donor.[49] We note that ESR signal in dark were reported in pentacene and picene films in FETs only after the application of a gate voltage, V_g.[50, 51] These observations suggest interesting transport properties which were not observed in other pentacene's host organic materials.

The resolved hyperfine quintet in the photo-ESR spectrum for $\theta \sim 80°$ in **Figure 2f** are ascribed to the dipole-dipole interaction between the triplet exciton and four equivalent protons of the pentacene molecule. This interpretation is supported by the simulation of the intensity pattern of the quintet 1-4-6-4-1. In addition, this result agrees with spin density calculations which

predict a distribution of the triplet over the ^{13}C nuclei in positions 6 (13) and 5 (7-12-14) (**Figure 1**). The simulation of the spectrum for $\theta \sim 80$ ° in **Figure 2f** to **Equation 1** assuming 4 equivalent ^{1}H atoms provides an isotropic hyperfine splitting $A_i \sim 4$ MHz whose summation is consistent with the hyperfine interaction A_{dip} calculated in dipole-dipole approximation adding all the contributions of 4 equivalent protons located at 0.25 nm from the centre of pentacene with the following formula:

$$A_{dip} = \sum_i \frac{\mu_0}{4\pi} \frac{\mu_B \mu_N g_e g_N}{h r_i^3} \quad (2)$$

where μ_0 is the vacuum permeability, μ_B is the Bohr magneton, μ_N is the nuclear Bohr magneton, g_e is the electron g factor, g_N is the nuclear g factor of hydrogen, h is Planck's constant, and r_i is the distance between the center of the pentacene molecule and each of the 4 equivalent hydrogen atom's groups.

The resolved hyperfine interaction reveals its dominant contribution to the overall peak-to-peak linewidth of the lowest resonance line (~ 1.5 mT). This result suggests that other contributions for instance due to triplet-triplet dipolar interactions occurs on an energy scale much lower than 4 MHz which corresponds to a triplet-triplet distance of ~ 4 nm. These results further corroborate the assumption that the four resonances observed in the photo-ESR spectra originate mainly from isolated triplets.

After photoexcitation, the occurrence of ISC leads to a fluorescence decreases for a time interval related to the resident time of electrons in the T_1 state. When the magnetic resonance condition is satisfied, the population of the T_1 sublevels labelled as T_x, T_y and T_z is changed, thus leading to a variation of the $T_1 \rightarrow S_0$ decay rates, and hence to an ODMR signal.[52] In the particular case of pentacene, T_x and T_y levels have shorter decay rates than T_z and microwave transitions $T_x \rightarrow T_z$ and $T_y \rightarrow T_z$ are induced leading to a longer life time of the T_1 state that causes a variation of the light emission intensity. [15, 45] In the presence of a magnetic field and crystal orientation, the T_x, T_y, T_z levels are mixed into a superposition of states and they are labelled as |0>, |+1> and |-1> .[17, 19, 53] The |0> state indicates the crystal orientation parallel to the applied magnetic field vector.

We observe a maximum ODMR contrast of about 15% for $\theta \sim 90°$, which slowly decreases for $90° < \theta < 50°$ and quickly vanishes for $\theta < 50°$, albeit reappearing for $\theta \sim 0°$. This trend is consistent with the angular dependent photo-ESR study shown in **Figure 2c** and confirm the mixing of the T_1 sublevels that changes the ESR transition probabilities. The values for the ODMR contrast are comparable to those reported for pentacene in *p*-terphenyl although at T =

1.8 K[54], and they are relatively high if compared to other organic molecules[55-59] and to those of inorganic systems such as silicon carbide [60] and NV centres in diamond where ODMR contrasts of 2% and 20% have been reported, respectively.[61] Therefore, our results support large inversion of population within the triplet state, a property relevant for nuclear spin polarization and quantum sensing applications.[17] Furthermore, we envisage that by exploiting the energy transfer from picene to pentacene,[33] the pentacene triplet exciton state could be excited by low excitation densities and high-energy lasers which will expand the range of potential applications on these compounds, particularly for the development of MASER technologies.[18]

Conclusion

We have reported on a new single crystal made by picene doped with pentacene and characterized its spin and angular dependent optical properties by ODMR and photo-ESR. We have detected the emissive and absorptive modes of the pentacene triplet exciton states and determined the zero-field splitting, the hyperfine interaction of the triplet exciton with four equivalent protons of the pentacene molecule as well as a dark ESR signal. Finally, we have observed a large ODMR contrast which can be tuned by crystal rotation.

Our findings demonstrate that isolated pentacene molecules in the picene matrix show efficient and tunable spin-dependent optical activities on a broad time-scale range spanning up to milliseconds. In addition, the observation of ESR signal in the absence of laser light illumination suggests interesting triplet transport properties which were not observed in other pentacene's host organic materials and as such deserve further investigations.

In perspective, we envisage that the optical transfer from picene to pentacene holds the potential to extend the excitation of the triplet exciton of pentacene in the ultraviolet region of the electromagnetic spectrum. These properties are particularly appealing for the exploitation of pentacene in spin-driven opto-electronics applications[62] and sensing[17] as well as in low power microwave amplification by stimulated emission of radiation (MASER). This is a research topic that we are currently pursuing.

Acknowledgements

We thank the University of Milano-Bicocca, the Materials and Spectroscopies for Nanoelectronics and Spintronics (MSNS) laboratory, the Swedish Interdisciplinary Magnetic

Resonance Centres (SIMARC) and the Italian MIUR through the Progetto Premiale 2012 "EOS: organic electronics for advanced research instrumentation". We thank Prof. W. M. Chen, Prof. M. Fanciulli and Dr T. Toccoli for reading the manuscript and useful comments.

Conflict of Interest

The authors declare no conflict of interest.

Data Availability

The datasets generated during and/or analysed during the current study are available in the Bicocca Open Archive Research Data repository, DOI: 10.17632/ncrnw9d3mg.1

References

1. K.J. Baeg, M. Binda, D. Natali, M. Caironi and Y.Y. Noh: Organic Light Detectors: Photodiodes and Phototransistors. *Adv. Mater.* **25**, 4267 (2013).
2. V.A. Dediu, L.E. Hueso, I. Bergenti and C. Taliani: Spin routes in organic semiconductors. *Nat. Mater.* **8**, 707 (2009).
3. K. Broch, J. Dieterle, F. Branchi, N.J. Hestand, Y. Olivier, H. Tamura, C. Cruz, V.M. Nichols, A. Hinderhofer, D. Beljonne, F.C. Spano, G. Cerullo, C.J. Bardeen and F. Schreiber: Robust singlet fission in pentacene thin films with tuned charge transfer interactions. *Nat. Commun.* **9** (2018).
4. D. Lubert-Perquel, E. Salvadori, M. Dyson, P.N. Stavrinou, R. Montis, H. Nagashima, Y. Kobori, S. Heutz and C.W.M. Kay: Identifying triplet pathways in dilute pentacene films. *Nat. Commun.* **9** (2018).
5. J. Girovsky, J. Nowakowski, E. Ali, M. Baljozovic, H.R. Rossmann, T. Nijs, E.A. Aeby, S. Nowakowska, D. Siewert, G. Srivastava, C. Wackerlin, J. Dreiser, S. Decurtins, S.X. Liu, P.M. Oppeneer, T.A. Jung and N. Ballav: Long-range ferrimagnetic order in a two-dimensional supramolecular Kondo lattice. *Nat. Commun.* **8** (2017).
6. M.C. Hanna and A.J. Nozik: Solar conversion efficiency of photovoltaic and photoelectrolysis cells with carrier multiplication absorbers. *J. Appl. Phys.* **100** (2006).
7. H. Kraus, M.C. Heiber, S. Vath, J. Kern, C. Deibel, A. Sperlich and V. Dyakonov: Analysis of Triplet Exciton Loss Pathways in PTB7: PC71BM Bulk Heterojunction Solar Cells. *Sci. Rep.* **6** (2016).
8. J.E. Anthony: The larger acenes: Versatile organic semiconductors. *Angew. Chem. Int. Ed.* **47**, 452 (2008).
9. H. Okamoto, N. Kawasaki, Y. Kaji, Y. Kubozono, A. Fujiwara and M. Yamaji: Air-assisted high-performance field-effect transistor with thin films of picene. *J. Am. Chem. Soc.* **130**, 10470 (2008).
10. G.A. Artioli, F. Hammerath, M.C. Mozzati, P. Carretta, F. Corana, B. Mannucci, S. Margadonna and L. Malavasi: Superconductivity in Sm-doped n phenacenes (n=3,4,5). *Chem. Commun.* **51**, 1092 (2015).
11. H.A. Galue, J. Oomens, W.J. Buma and B. Redlich: Electron-flux infrared response to varying pi-bond topology in charged aromatic monomers. *Nat. Commun.* **7** (2016).
12. Y. Kubozono, H. Mitamura, X. Lee, X.X. He, Y. Yamanari, Y. Takahashi, Y. Suzuki, Y. Kaji, R. Eguchi, K. Akaike, T. Kambe, H. Okamoto, A. Fujiwara, T. Kato, T. Kosugi and H. Aoki: Metal-intercalated aromatic hydrocarbons: a new class of carbon-based superconductors. *Phys. Chem. Chem. Phys.* **13**, 16476 (2011).

13. M. Bendikov, F. Wudl and D.F. Perepichka: Tetrathiafulvalenes, oligoacenenes, and their buckminsterfullerene derivatives: The brick and mortar of organic electronics. *Chem. Rev.* **104**, 4891 (2004).
14. P. Cudazzo, M. Gatti and A. Rubio: Excitons in molecular crystals from first-principles many-body perturbation theory: Picene versus pentacene. *Phys. Rev. B* **86** (2012).
15. J. Wrachtrup, C. Vonborczyskowski, J. Bernard, M. Orrit and R. Brown: Optically detected spin coherence of single molecues *Phys. Rev. Lett.* **71**, 3565 (1993).
16. M. Orrit and J. Bernard: Sinlge pentacene molecules detected by fluorescence in a para terphenyl crystal *Phys. Rev. Lett.* **65**, 2716 (1990).
17. K. Tateishi, M. Negoro, S. Nishida, A. Kagawa, Y. Morita and M. Kitagawa: Room temperature hyperpolarization of nuclear spins in bulk. *Proc. Natl. Acad. Sci. U.S.A.* **111**, 7527 (2014).
18. M. Oxborrow, J.D. Breeze and N.M. Alford: Room-temperature solid-state maser. *Nature* **488**, 353 (2012).
19. D.J. Sloop, H.L. Yu, T.S. Lin and S.I. Weissman: Electron spin echoes of a photoexcited triplet pentacene in paraterphenyl crystals. *J. Chem. Phys.* **75**, 3746 (1981).
20. A. Henstra, T.S. Lin, J. Schmidt and W.T. Wenckebach: High dynamic nuclear polarization at room temperature. *Chem. Phys. Lett.* **165**, 6 (1990).
21. A. Kagawa, M. Negoro, R. Ohba, N. Ichijo, K. Takamine, Y. Nakamura, T. Murata, Y. Morita and M. Kitagawa: Dynamic Nuclear Polarization using Photoexcited Triplet Electron Spins in Eutectic Mixtures. *J. Phys. Chem. A* **122**, 9670 (2018).
22. O.D. Jurchescu, J. Baas and T.T.M. Palstra: Effect of impurities on the mobility of single crystal pentacene. *Appl. Phys. Lett.* **84**, 3061 (2004).
23. C. Reese, W.J. Chung, M.M. Ling, M. Roberts and Z.N. Bao: High-performance microscale single-crystal transistors by lithography on an elastomer dielectric. *Appl. Phys. Lett.* **89** (2006).
24. P.M. Zimmerman, Z.Y. Zhang and C.B. Musgrave: Singlet fission in pentacene through multi-exciton quantum states. *Nat. Chem.* **2**, 648 (2010).
25. A. Rao, M.W.B. Wilson, J.M. Hodgkiss, S. Albert-Seifried, H. Bassler and R.H. Friend: Exciton Fission and Charge Generation via Triplet Excitons in Pentacene/C-60 Bilayers. *J. Am. Chem. Soc.* **132**, 12698 (2010).
26. H. Najafov, B. Lee, Q. Zhou, L.C. Feldman and V. Podzorov: Observation of long-range exciton diffusion in highly ordered organic semiconductors. *Nat. Mater.* **9**, 938 (2010).
27. H. Okamoto, S. Hamao, R. Eguchi, H. Goto, Y. Takabayashi, P.Y.H. Yen, L.U. Liang, C.W. Chou, G. Hoffmann, S. Gohda, H. Sugino, Y.F. Liaos, H. Ishii and Y. Kubozono: Synthesis of the extended phenacene molecules, 10 phenacene and 11 phenacene, and their performance in a field-effect transistor. *Sci. Rep.* **9** (2019).
28. R. Mitsuhashi, Y. Suzuki, Y. Yamanari, H. Mitamura, T. Kambe, N. Ikeda, H. Okamoto, A. Fujiwara, M. Yamaji, N. Kawasaki, Y. Maniwa and Y. Kubozono: Superconductivity in alkali-metal-doped picene. *Nature* **464**, 76 (2010).
29. S. Gottardi, T. Toccoli, S. Iannotta, P. Bettotti, A. Cassinese, M. Barra, L. Ricciotti and Y. Kubozono: Optimizing Picene Molecular Assembling by Supersonic Molecular Beam Deposition. *J. Phys. Chem. C* **116**, 24503 (2012).
30. Y. Shimo, T. Mikami, H.T. Murakami, S. Hamao, H. Goto, H. Okamoto, S. Gohda, K. Sato, A. Cassinese, Y. Hayashi and Y. Kubozono: Transistors fabricated using the single crystals of 8 phenacene. *J. Mater. Chem. C* **3**, 7370 (2015).
31. T. Taguchi, F. Chiarella, M. Barra, F. Chianese, Y. Kubozono and A. Cassinese: Balanced Ambipolar Charge Transport in Phenacene/Perylene Heterojunction-Based Organic Field-Effect Transistors. *ACS Appl. Mater. Interfaces* **13**, 8631 (2021).
32. T. Hosokai, A. Hinderhofer, F. Bussolotti, K. Yonezawa, C. Lorch, A. Vorobiev, Y. Hasegawa, Y. Yamada, Y. Kubozoro, A. Gerlach, S. Kera, F. Schreiber and N. Ueno: Thickness and Substrate

Dependent Thin Film Growth of Picene and Impact on the Electronic Structure. *J. Phys. Chem. C* **119**, 29027 (2015).
33. T. Toccoli, P. Bettotti, A. Cassinese, S. Gottardi, Y. Kubozono, M.A. Loi, M. Manca and R. Verucchi: Photophysics of Pentacene-Doped Picene Thin Films. *J. Phys. Chem. C* **122**, 16879 (2018).
34. A. De, R. Ghosh, S. Roychowdhury and P. Roychowdhury: Structural-analysis of picene, $C_{22}H_{14}$. *Acta Crystallogr. Sect. C: Cryst. Struct. Commun.* **41**, 907 (1985).
35. T. Siegrist, C. Kloc, J.H. Schon, B. Batlogg, R.C. Haddon, S. Berg and G.A. Thomas: Enhanced physical properties in a pentacene polymorph. *Angew. Chem. Int. Ed.* **40**, 1732 (2001).
36. J.A. Rackers, Z. Wang, C. Lu, M.L. Laury, L. Lagardere, M.J. Schnieders, J.P. Piquemal, P.Y. Ren and J.W. Ponder: Tinker 8: Software Tools for Molecular Design. *J. Chem. Theory Comput.* **14**, 5273 (2018).
37. W.L. Jorgensen, D.S. Maxwell and J. Tirado-Rives: Development and Testing of the OPLS All-Atom Force Field on Conformational Energetics and Properties of Organic Liquids. *J. Am. Chem. Soc.* **118**, 11225 (1996).
38. W.L. Jorgensen and J. Tirado-Rives: Potential energy functions for atomic-level simulations of water and organic and biomolecular systems. *Proc. Natl. Acad. Sci. U.S.A.* **102**, 6665 (2005).
39. S. Stoll and A. Schweiger: EasySpin, a comprehensive software package for spectral simulation and analysis in EPR. *J. Magn. Reson.* **178**, 42 (2006).
40. B. Mahns, O. Kataeva, D. Islamov, S. Hampel, F. Steckel, C. Hess, M. Knupfer, B. Buchner, C. Himcinschi, T. Hahn, R. Renger and J. Kortus: Crystal Growth, Structure, and Transport Properties of the Charge-Transfer Salt Picene/2,3,5,6-Tetrafluoro-7,7,8,8-tetracyanoquinodimethane. *Cryst. Growth Des.* **14**, 1338 (2014).
41. Z.S. Zhao, L.H. Britt and G.K. Murphy: Oxidative, Iodoarene-Catalyzed Intramolecular Alkene Arylation for the Synthesis of Polycyclic Aromatic Hydrocarbons. *Chem. Eur. J.* **24**, 17002 (2018).
42. J. Lang, D.J. Sloop and T.S. Lin: Orientational anisotropic studies by field rotation technique: Near zero-field pulsed EPR experiments of pentacene doped in p-terphenyl. *J. Magn. Reson.* **176**, 249 (2005).
43. J. Dieterle, K. Broch, A. Hinderhofer, H. Frank, J. Novak, A. Gerlach, T. Breuer, R. Banerjee, G. Witte and F. Schreibert: Structural Properties of Picene-Perfluoropentacene and Picene-Pentacene Blends: Super lattice Formation versus Limited Intermixing. *J. Phys. Chem. C* **119**, 26339 (2015).
44. N. Hirota, M. Baba, Y. Hirata and S. Nagaoka: ODMR AND EPR STUDIES OF THE TRIPLET-STATES OF ALIPHATIC AND AROMATIC CARBONYLS. *J. Phys. Chem.* **83**, 3350 (1979).
45. J. Kohler, A.C.J. Brouwer, E.J.J. Groenen and J. Schmidt: FLUORESCENCE DETECTION OF SINGLE-MOLECULE MAGNETIC-RESONANCE FOR PENTACENE IN P-TERPHENYL - THE HYPERFINE INTERACTION OF A SINGLE TRIPLET SPIN WITH A SINGLE C-13 NUCLEAR-SPIN. *Chem. Phys. Lett.* **228**, 47 (1994).
46. T. Yago, G. Link, G. Kothe and T.S. Lin: Pulsed electron nuclear double resonance studies of the photoexcited triplet state of pentacene in p-terphenyl crystals at room temperature. *J. Chem. Phys.* **127** (2007).
47. S.S. Kim: Triplet state of picene in para terphenyl crystals by EPR. *Chem. Phys. Lett.* **61**, 327 (1979).
48. H.L. Yu, T.S. Lin, S.I. Weissman and D.J. Sloop: Time resolved studies of pentacene triplets by electron spin echo spectroscopy. *J. Chem. Phys.* **80**, 102 (1984).
49. B. Balambiga, R. Dheepika, P. Devibala, P.M. Imran and S. Nagarajan: Picene and PTCDI based solution processable ambipolar OFETs. *Sci. Rep.* **10** (2020).
50. T. Oyama, Y.S. Yang, K. Matsuo and T. Yasuda: Effects of chalcogen atom substitution on the optoelectronic and charge-transport properties in picene-type pi-systems. *Chem. Commun.* **53**, 3814 (2017).

51. K. Marumoto, S. Kuroda, T. Takenobu and Y. Iwasa: Spatial extent of wave functions of gate-induced hole carriers in pentacene field-effect devices as investigated by electron spin resonance. *Phys. Rev. Lett.* **97** (2006).
52. P.G. Baranov, H.J. von Bardeleben, F. Jelezko and J. Wrachtrup: Magnetic Resonance of Semiconductors and Their Nanostructures: Basic and Advanced Applications, (Springer Vienna2017).
53. T.C. Yang, D.J. Sloop, S.I. Weissman and T.S. Lin: Magnetic effects on the dynamics of organic triplets in the level anti-crossing region. *Mol. Phys.* **100**, 1333 (2002).
54. R. Brown, J. Wrachtrup, M. Orrit, J. Bernard and C. Vonborczyskowski: Kinetics of optically detected magnetic-resonance of single molecules. *J. Chem. Phys.* **100**, 7182 (1994).
55. L.S. Swanson, P.A. Lane, J. Shinar and F. Wudl: Polarons and triplet excitons in poly(paraphenylene)(PPV) and substitued PPV. An optically detected magnetic resonance study. *Phys. Rev. B* **44**, 10617 (1991).
56. V. Dyakonov, N. Gauss, G. Rosler, S. Karg and W. Riess: Electron spin resonance in PPV photodiodes detection via photoinduced current. *Chem. Phys.* **189**, 687 (1994).
57. J. De Ceuster, E. Goovaerts, A. Bouwen and V. Dyakonov: Recombination of triplet excitons and polaron pairs in a derived paraphenylene vinylene pentamer. *Phys. Rev. B* **68** (2003).
58. J. Shinar and J. Partee: On the nature of trapped polarons in pi-conjugated polymers. *Synth. Met.* **84**, 525 (1997).
59. P.A. Lane, L.S. Swanson, Q.X. Ni, J. Shinar, J.P. Engel, T.J. Barton and L. Jones: Dynamics of photoexticed states in $C_{60.}$ An optically deteced magnetic resonance, ESR and light induced ESR study. *Phys. Rev. Lett.* **68**, 887 (1992).
60. J.F. Wang, J.M. Cui, F.F. Yan, Q. Li, Z.D. Cheng, Z.H. Liu, Z.H. Lin, J.S. Xu, C.F. Li and G.C. Guo: Optimization of power broadening in optically detected magnetic resonance of defect spins in silicon carbide. *Phys. Rev. B* **101** (2020).
61. E.V. Levine, M.J. Turner, P. Kehayias, C.A. Hart, N. Langellier, R. Trubko, D.R. Glenn, R.R. Fu and R.L. Walsworth: Principles and techniques of the quantum diamond microscope. *Nanophotonics* **8**, 1945 (2019).
62. T.D. Nguyen, E. Ehrenfreund and Z.V. Vardeny: Spin-Polarized Light-Emitting Diode Based on an Organic Bipolar Spin Valve. *Science* **337**, 204 (2012).